

# Climate Anomalies Induced by the Arctic and Antarctic Oscillations: Glacial Maximum and Present-Day Perspectives

F. JUSTINO\* AND W. R. PELTIER

*Department of Physics, University of Toronto, Toronto, Ontario, Canada*

(Manuscript received 29 September 2006, in final form 20 June 2007)

## ABSTRACT

Based on multicentury coupled climate simulations of both modern and glacial maximum conditions, this study focuses on the impact of the Arctic Oscillation (AO) and the Antarctic Oscillation (AAO) on the earth's surface climate. Intercomparison of the results obtained in numerical experiments for both climate epochs demonstrates that highly significant changes of surface climate are predicted to have occurred depending upon the phase of the AO and AAO. These climate anomalies differ substantially between the modern and Last Glacial Maximum (LGM) states and exhibit a strong seasonal cycle under the latter conditions. Additional investigation has revealed that an intensification of the subtropical gyres in the North Atlantic and North Pacific that are induced during the positive phase of the AO plays a key role in the development of positive sea surface temperature (SST) anomalies in midlatitudes. In the Southern Hemisphere, similarly significant and systematic climate shifts are shown to occur due to variations of the Antarctic Oscillation that are highlighted by a warming over the Antarctic Peninsula and midlatitudes during the positive phase of the AAO. Finally, the authors find that the temporal variability of the AO and of the Pacific decadal oscillation (PDO) is significantly anticorrelated, with this coupling being independent of the season under present-day conditions. Under LGM conditions, however, due to the intensified vigor of the atmospheric circulation, the coupling is found to be stronger during boreal winter.

## 1. Introduction

Over midlatitudes and the Northern Hemisphere (NH) polar region, the present-day climate regime is mainly dictated by vacillation in the phase of the Arctic Oscillation (AO; e.g., Rogers 1990; Wallace and Gutzler 1981). The AO is characterized by the existence of a well-known tripolar structure over the NH, which is dominated by two areas of strongest out-of-phase variability located over the polar region (Iceland) and midlatitudes (Azores). The impact of the AO on the variability of present-day surface climate conditions has been increasingly explored in several publications (e.g., Wang et al. 2005; Rodwell et al. 1999; Rogers 1990; Wallace and Gutzler 1981). According to Thompson and Wallace (2001), the AO affects not only mean

conditions but also the day-to-day variability of the weather regime, modulating the intensity of mid-latitude storms and the frequency of occurrence of high-latitude blocking and cold-air outbreaks throughout the NH. Observation-based analyses have revealed, furthermore, that surface temperatures over the NH extratropics in winter during the last two decades are higher now than at any other time over the past millennium, and this has been attributed to a positive trend of the AO index (Thompson and Wallace 2001; Hurrell 1995). Cook (2003) and Cook et al. (1998) have also highlighted the implications and importance of AO variability for proxy-based climate reconstructions, in particular for the Eurasian/Scandinavian region.

At high and midlatitudes in the Southern Hemisphere (SH), the climate regime is tightly linked to another mode of climate variability, namely, the Antarctic Oscillation (AAO; Gong and Wang 1999). This dominant pattern of climate variability exhibits a well-defined annular structure, which is defined by two areas of strongest out-of-phase variability located over midlatitudes (40°–55°S) and the polar region (Gong and Wang 1999). The AAO appears to be linked to latitu-

---

\* Current affiliation: Departamento de Engenharia Agrícola, Universidade Federal de Viçosa, MG, Brazil.

---

Corresponding author address: F. Justino, P.H. Rolfs, S/N, Centro, Vicosa 36570, Brazil.  
E-mail: fjustino@ufv.br

dinal migration of the subtropical upper-level jet and to variations in the intensity of the polar jet (Carvalho et al. 2005). In addition, the positive phase of the AAO is associated with the intensification of an upper-level anticyclonic anomaly, weakened moisture convergence, and decreased precipitation over southeastern South America (Silvestri and Vera 2003). Modeling results, moreover, have suggested that a positive trend of the AAO with an increasing midlatitude mean sea level pressure (SLP; Cai et al. 2005) is accompanied by multi-decadal fluctuations of winter rainfall over southwest Australia. Based on observational data, Thompson and Solomon (2002) presented additional evidence that recent trends in the SH tropospheric circulation can be interpreted as a bias toward the positive phase of the AAO. Oscillations of the AAO are also associated with lower SST and sea ice anomalies due to induced changes of the Ekman dynamics (Lefebvre et al. 2004; Hall and Visbeck 2002) of the Southern Ocean circulation.

The earth's climate during the Last Glacial Maximum (LGM; approximately 21 000 yr before present) was strongly affected by the modification of the mechanical forcing associated with the marked change in surface topography and by the thermal forcing related to enhanced ice albedo feedback. This raises the possibility of the existence of distinct polar climate variability under LGM conditions. Indeed, through the analysis of a sequence of coupled atmosphere–ocean climate simulations, Justino and Peltier (2005) demonstrated that the spatial and temporal variability of the AO is expected to have been drastically different under glacial boundary conditions compared to today. They show that while during the positive phase of the modern AO a strong westerly flow develops over the Atlantic Ocean, in the glacial northern mode (GNM) enhanced southerly wind anomalies act over this region, whereas cyclonic winds dominate the atmospheric flow over Siberia. Hereafter, the AO as predicted by the LGM simulation will be referred to as the GNM. These modifications of north polar climate variability are expected to result in significant changes of surface climate conditions depending upon the phase of the AO under LGM conditions. In a further recent study, Justino and Peltier (2006) have similarly investigated the impact of glacial boundary conditions on the SH mode of climate variability, analyses that led them to identify a glacial southern mode (GSM). They demonstrate that, despite substantial climate anomalies in the polar region in the summer season in the LGM simulation, no prominent change in the spatial structure of the mode, as compared to the modern Southern Hemisphere annular mode (SAM), would be expected. Dur-

ing the winter season, however, this mode was shown to have been drastically modified at LGM due to a substantial change of SH polar climate symmetry.

An investigation of the global patterns of natural climate variability associated with the AO and AAO is, therefore, a prerequisite background to the understanding of regional features due to the continuing action of greenhouse gas-induced global warming. A detailed analysis of this source of variability in climate anomaly patterns is also expected to shed some light upon the cause of discrepancies between proxy data-based reconstructions for critical times in the distant past due to AO and AAO local vacillations. Our goal in the present paper is to provide a further evaluation from a global perspective of the impacts of the AO and AAO under modern and LGM conditions, on both the atmospheric general circulation and on land and sea surface conditions. This is motivated by the fact that these changes in the structure of extratropical climate variability will have to be carefully considered when temperature, large-scale circulation, or precipitation/snowfall is estimated from paleoproxy data for the LGM interval. Although this is an important issue, no previous attempt has been made to systematically investigate the impact of the AO and AAO on the LGM climate regime. The paper is organized as follows: Section 2 describes the coupled atmosphere–ocean–sea ice model, the design of the experiments to be analyzed, and an intercomparison between modeling results and paleo-proxy-based reconstructions. In section 3, the climate impacts induced by the AO and AAO under both present-day and glacial conditions are described. This section also includes a brief discussion of the coupling between the AO and the Pacific decadal oscillation (PDO). Section 4 summarizes our main findings.

## 2. The coupled climate model and the design of the numerical experiments

The coupled atmosphere–ocean–sea ice model employed in this study is the National Center for Atmospheric Research (NCAR) Climate System Model (CSM). The atmospheric general circulation component of the model that we employ is the low-resolution version of CSM1.4 that incorporates 18 vertical levels in the atmosphere in which the model fields are truncated triangularly at degree and order 31, which corresponds to  $96 \times 48$  longitude and latitude grid points (Kiehl et al. 1998). The dynamics of the ocean are described on 25 vertical levels on a  $3^\circ \times 3^\circ$  grid. Additionally, the coupled model includes a sophisticated sea ice component (Bettge et al. 1996) as well as a simplified representation of land surface processes (Bonan 1998).

The NCAR CSM model has been extensively used to simulate the present-day climate and no purpose will be served by discussing this in detail herein. To investigate the main modes of climate variability, as well as their impact on mean climate state, two model simulations have been performed, an experiment driven by present-day boundary conditions (MOD) and a second experiment for the LGM (Peltier and Solheim 2004). The MOD (LGM) simulation was run to equilibrium for 2000 (2500) yr (Peltier and Solheim 2004), and the analyses discussed herein are based upon the last 500 yr of each simulation. We focus on the winter [December–February (DJF)] and summer [June–August (JJA)] seasons. In the LGM simulation, we set the four major boundary conditions that are required for the purpose of such analyses as follows: (i) orbital parameters were fixed to those corresponding to 21 000 yr ago, (ii) ice sheet topography and albedo were fixed according to the ICE-4G model (Peltier 1994), (iii) the land–sea mask and paleo–sea level were also fixed according to the ICE-4G model, and (iv) the concentrations of the radiatively active atmospheric trace gases ( $\text{CO}_2$ ,  $\text{CH}_4$ , and  $\text{N}_2\text{O}$ ) are also to be adjusted based upon estimates from the Vostok ice core. Specifically, these concentrations were taken to be 200 ppmv for  $\text{CO}_2$ , 400 ppbv for  $\text{CH}_4$ , and 275 ppbv for  $\text{N}_2\text{O}$ .

This study provides a first investigation, based upon the use of a state-of-the-art coupled climate model, of the impact of the GNM and GSM on the earth's surface conditions.

#### *The intercomparison between the simulated glacial climate and proxy-based reconstructions*

Peltier and Solheim (2004) have provided a detailed and in-depth analysis of the oceanic conditions delivered by the LGM and MOD simulations. Moreover, they presented an extensive intercomparison between the model results and paleoreconstructions in which it is demonstrated that the simulated LGM climate is in close accord with most recent paleoceanographic inferences. To provide an intercomparison between the glacial oceanic conditions (SST and sea ice extent) and currently available paleoreconstructions, Fig. 1a shows the simulated SST anomalies between the LGM and MOD simulations based upon the CSM1.4 model. In Fig. 1b, we present the annually averaged SST anomalies between the Levitus climatology (Levitus 1982) and the Glacial Atlantic Ocean Mapping (GLAMAP; Pflaumann et al. 2003) project. The GLAMAP dataset presents a new reconstruction of SST, sea surface salinity (SSS), and sea ice margins for the North and South Atlantic during the LGM period. The GLAMAP reconstruction for the Atlantic is based on the analysis

of 275 sediment cores located between the North Pole and 60°S.

Figures 1a and 1b show that, on basin scale, SST anomalies between the LGM and MOD simulations (Fig. 1b) are in good agreement with the GLAMAP–Levitus anomalies, in particular in the North Atlantic where the magnitude of the SST anomalies reaches values as high as  $-10^\circ\text{C}$ . Similarly, in the SH extratropics the model and paleoreconstructions are also in reasonably close agreement. The high degree of similarity between these anomalies in the western Atlantic along the east coast of the South American continent is especially apparent. In the tropical region (30°N–30°S), however, the model is about  $1^\circ\text{C}$  colder than the GLAMAP reconstructions (Figs. 1a,b). It should be noted that no attempt was made to incorporate the influence of atmospheric aerosols in the LGM integration (Peltier and Solheim 2004), which may be the cause of the intensified tropical cooling. From Figs. 1c and 1d, it is evident that a substantial increase of sea ice extent in the NH under LGM conditions is predicted by the model with the southern boundary of essentially perennial sea ice markedly shifted to lower latitudes [this result is similar to the Climate: Long-Range Investigation, Mapping, and Prediction (CLIMAP) reconstruction (CLIMAP 1981)]. Compared to the GLAMAP, inferences are clear that the LGM simulation overestimates the sea ice distribution in both seasons but particularly in NH winter (Fig. 1c). This seems to be associated with the large amount of heat transferred from the ocean to the much colder atmosphere, which in turn induces oceanic cooling and sea ice formation. On the other hand, Fig. 1d shows that in JJA the model and reconstructions are in much better agreement in the SH.

Turning to a discussion of the changes in surface temperature at 2 m (Fig. 1e), due to the inclusion of glacial boundary conditions, it is found that the annually and globally averaged surface temperature in the LGM simulation equilibrates at a level of  $9.6^\circ\text{C}$ , which is about  $6^\circ\text{C}$  lower than in the MOD simulation (Peltier and Solheim 2004). Several studies (e.g., Justino et al. 2005; Shin et al. 2003; Vettoretti et al. 2000; Rind 1987; Manabe and Broccoli 1985) have attributed a significant portion of the LGM cooling to the mechanical and diabatic influence of glacial topography and albedo forcing. Moreover, Kim et al. (2003) and Broccoli and Manabe (1987) have demonstrated that the reduction of the atmospheric  $\text{CO}_2$  concentration characteristic of glacial conditions also plays an important role in controlling the tropical and SH cooling. Compared to the MOD simulation (Fig. 1e), the regional cooling in the LGM simulation exceeds  $-20^\circ\text{C}$  from North America to Eurasia primarily as a consequence of the lapse rate

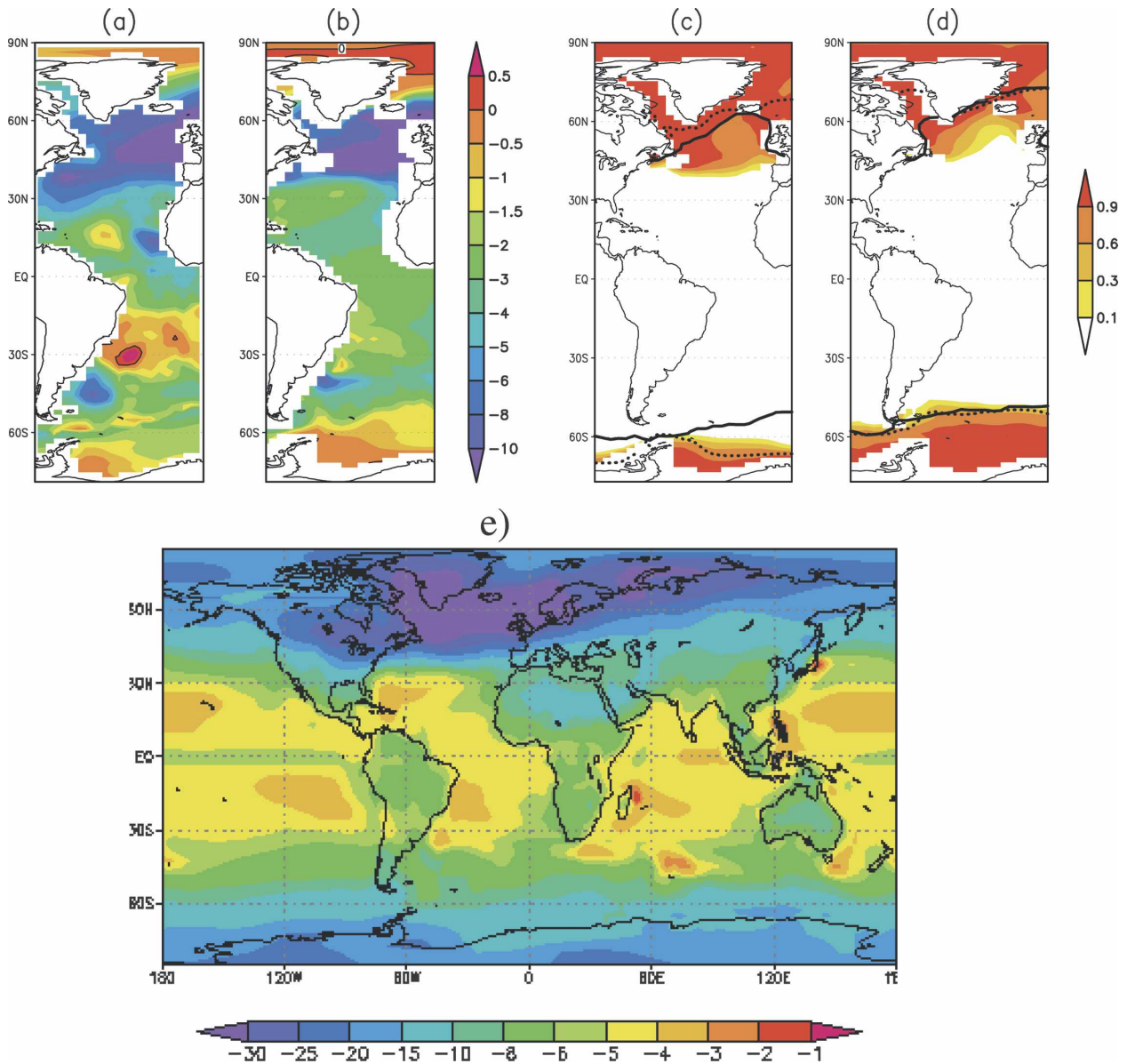


FIG. 1. (a) Time-averaged SST differences between the LGM and MOD simulations. (b) The SST anomalies between the GLAMAP reconstruction and present-day SST from Levitus (1982) ( $^{\circ}\text{C}$ ). The black curve is the OK. The sea ice margin in the LGM experiment (shaded) and reconstructed from GLAMAP (thick line) for (c) February and (d) August. The dotted line depicts simulated present-day conditions. The lines bound values of sea ice concentration in the grid cell larger than 0.1. (e) Surface temperature anomalies at 2 m between the MOD and LGM simulations.

effect due to the enhanced topography associated with the continental ice cover. Surface albedo changes and increased sea ice extent further contribute to the glacial cooling. Surface temperature anomalies in the tropical region are smaller, by up to  $-7^{\circ}\text{C}$  over the continents and by up to  $-5^{\circ}\text{C}$  over the oceans.

To continue with our evaluation of the quality of the modeling results based upon intercomparison with proxy-based reconstructions, Fig. 2 shows the predicted

LGM anomalies for the temperature of the coldest month (TCOLD), the temperature of the warmest month (TWARM), and the annual mean precipitation (PPT). These quantities are compared to climate anomalies based upon the reconstructions by Peyron et al. (2005) and Tarasov et al. (1999). First, it is important to identify possible model bias in the predicted present-day climate. It is evident based on Figs. 2a and 2b that compared to National Centers for Environmen-

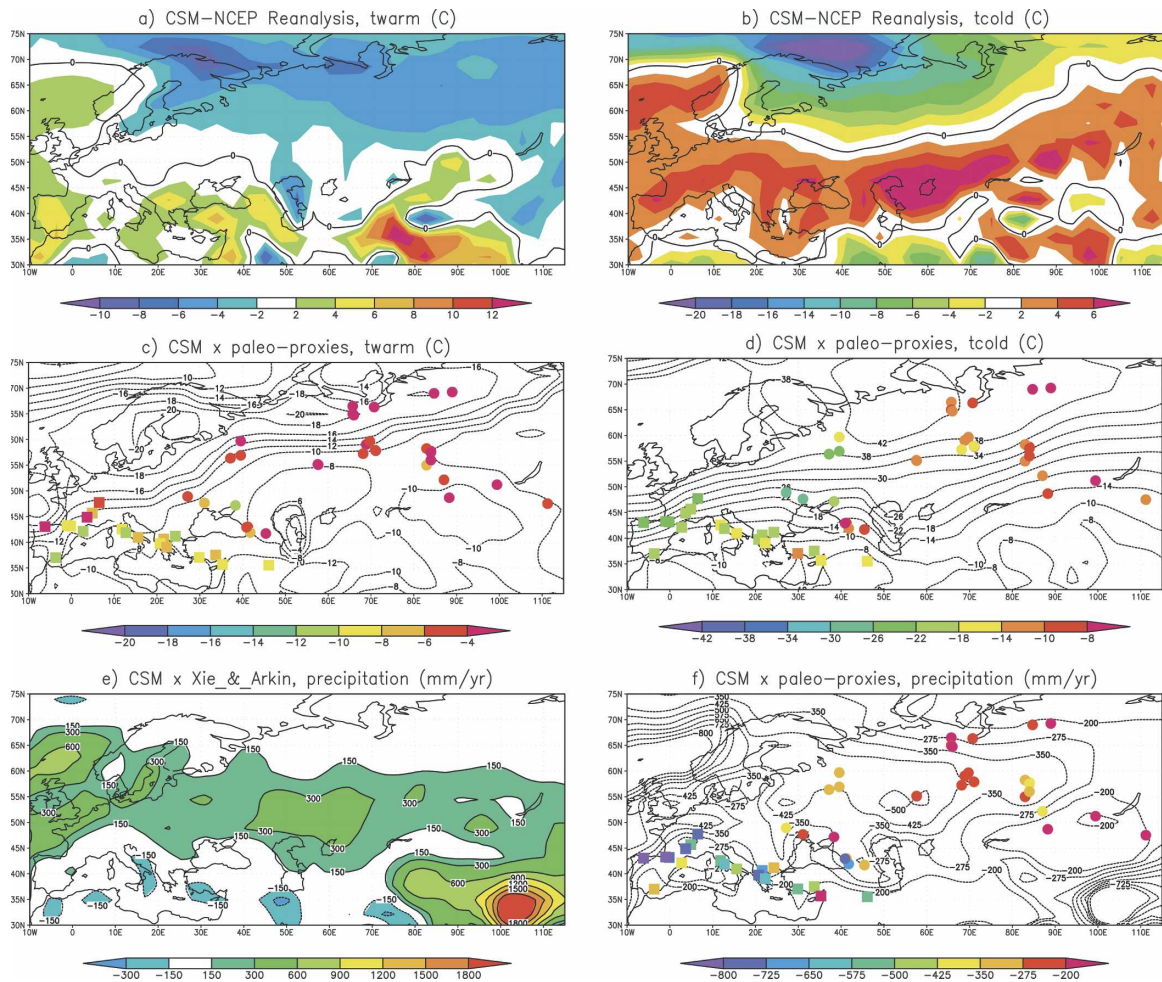


FIG. 2. (a) Temperature anomalies ( $^{\circ}\text{C}$ ) of the warmest month between the MOD simulation and NCEP reanalyses. (b) Same as (a) but for the coldest month. (c), (d) The LGM mean temperature anomalies of the warmest and coldest month (contour) as compared to the MOD simulation. Respective climate anomalies as reconstructed by Tarasov et al. (1999) and Peyron et al. (2005) are shown by squares and dots. (e) Annually averaged precipitation anomalies between MOD simulation and Xie and Arkin (1997). (f) Time-averaged precipitation anomalies between MOD and LGM simulations (contour) and the climate reconstructions according to Tarasov et al. (1999) and Peyron et al. (2005).

tal Prediction (NCEP) data our MOD simulation predicts lower TWARM (MOD - NCEP) and TCOLD (MOD - NCEP) for Eurasia/Scandinavia and the Nordic Seas, whereas warmer conditions are simulated over central Europe. Therefore, the CSM version 1.4 model exhibits a cold (warm) bias over high latitudes (subtropics) under present-day conditions. Turning to the paleomodeling analyses (Figs. 2c,d), a different picture emerges. The comparison between the simulated TWARM (LGM-MOD) anomalies and the pollen-based reconstructions reveals that the model reproduces satisfactorily the proxy data over the southern Europe/Mediterranean region (Fig. 2c). It is also clear that the modeled TWARM (LGM-MOD) anomalies are much colder elsewhere than suggested by

the palynology. Similar bias is also noted in the TCOLD (LGM-MOD) anomalies (Fig. 2d). This discrepancy between model results and reconstructions over high latitudes is perhaps arising due to the presence of the Fennoscandia ice sheet. The ICE-4G paleogeography employed in the analyses reported here (Peltier 1994) extends farther to the south and east and then is consistent with the most recent glaciological data, thus increasing the surface albedo and the downstream advection of cold air in the lee of the Eurasian ice complex. Furthermore, it is important to recall that the considerable increase in sea ice extent under LGM conditions in the North Atlantic is another forcing responsible for additional cooling in northern Europe.

TABLE 1. Mean temperature anomalies of the coldest month ( $\Delta$ TCOLD) between LGM and MOD simulations over equatorial South America (ESA; 10°N–2°S, 50°–75°W), equatorial East Africa (EEA; 10°N–10°S, 25°–45°E), New Guinea (NG; 0°–10°S, 130°–150°E), subtropical South Africa (SSA; 15°–35°S, 15°–35°E), and subtropical eastern North America (SENA; 30°–35°N, 75°–85°W). The minimum and maximum represent the minimum and maximum  $\Delta$ TCOLD within the regions among the proxy data. The table is derived from Shin et al. (2003).

$\Delta$ TCOLD	NCAR CSM (Shin et al. 2003)	ECBilt-CLIO (Justino et al. 2005)	Present paper area average	Farrera et al. (1999) min/max
ESA	–3.5	–3.0	–6.2	–3.0/–8.0
EEA	–3.5	–1.9	–6.8	–3.0/–5.0
NG	–3.6	–1.2	–5.6	–2.0/–7.0
SSA	–5.0	–2.4	–5.0	–3.7/–6.5
SENA	–4.4	–1.9	–11.0	–7.5/–15.5

To investigate precipitation anomalies, we first compare our simulated present-day precipitation with the Xie and Arkin (1997) dataset (Fig. 2e). This demonstrates that our modern climate overestimates the precipitation in central Europe, southeastern Asia, and in the North Atlantic. Elsewhere, model results and observations show anomalies between 150 and  $-150 \text{ mm yr}^{-1}$ , which represent differences smaller than  $1 \text{ mm day}^{-1}$ . Turning to the paleoreconstructions modeling evaluation, the analyses for precipitation (Fig. 2f), in contrast to temperature, reveal that the model results and paleoreconstructions are in considerably better agreement in the extratropical region, northward of 50°N. In the subtropical region, however, simulated LGM climate is too arid. This is likely a result of extremely cold conditions in the North Atlantic, which in turn reduces the evaporation, and the amount of water vapor that is embedded in the maritime air advected over the subtropical region. Changes in the form of the AO, as will be discussed below, may also play a significant role in generating these climate anomalies. It is a fundamental issue as to whether proper allowance is made in the proxy reconstructions for the impact of AO-induced variability.

To provide an initial intercomparison between our results and both previous LGM simulations (Justino et al. 2005; Shin et al. 2003) and paleoreconstructions of land surface temperatures (Farrera et al. 1999), Table 1 lists the mean temperature anomalies of TCOLD between the MOD and LGM simulations. Farrera et al. (1999) suggest that, during the LGM, TCOLD was between 3° and 15°C lower than at present in the tropical region (32°S–32°N). Comparison of our simulated temperatures with the paleoreconstructions reveals good agreement in the equatorial zone and over the subtropics (Table 1). However, the magnitude of the cooling is not uniformly distributed. For instance, northeastern Brazil, northwestern South America, and southeastern North America are predicted to have cooled by more than 5°C. This feature is well reproduced in our LGM

simulation. It should be noted that our results suggest much colder conditions than simulated by the other two LGM simulations, demonstrating that our results are in better agreement with the paleoreconstructions. Although Shin et al. (2003) employed the same version of CSM as in this study, their results may be somewhat compromised by the manner in which they forced the model to statistical equilibrium, since a deep-water acceleration scheme was employed for this purpose to reduce the computing time required to complete the simulation. It is well known that this approach is not energy conserving (Nakano et al. 1999) and that it may therefore lead to a distinct climate equilibrium and regional climate bias.

### 3. Polar modes of climate variability

Based on empirical orthogonal function (EOF) and spectral analysis performed on monthly data and in agreement with previous studies (e.g., Thompson and Wallace 2000; Kushner et al. 2001), the model-predicted AO and AAO are herein first displayed in terms of the spatial pattern of their amplitude, obtained by regressing the hemispheric geopotential height at 500-hPa (Z500) anomalies upon the monthly leading principal component (PC) time series from the hemispheric domain between 20° and 88° latitude. The 500-hPa geopotential height level was chosen to avoid intersection with planetary topography. However, it is found that there is no substantial difference in the EOF pattern if the analysis is performed at lower atmospheric levels (not shown). Figure 3 shows that the AO under modern conditions is dominated by two areas of strongest out-of-phase variability located over midlatitudes and the polar region. It is equally clear that within these areas nodes of distinct intensity do exist. One should note that our first EOF differs from the pattern obtained by Thompson and Wallace (1998), in the sense that the latter study predicted a more zonally elongated center of action over the East Asia/North Pacific sector. This discrepancy may arise from differ-

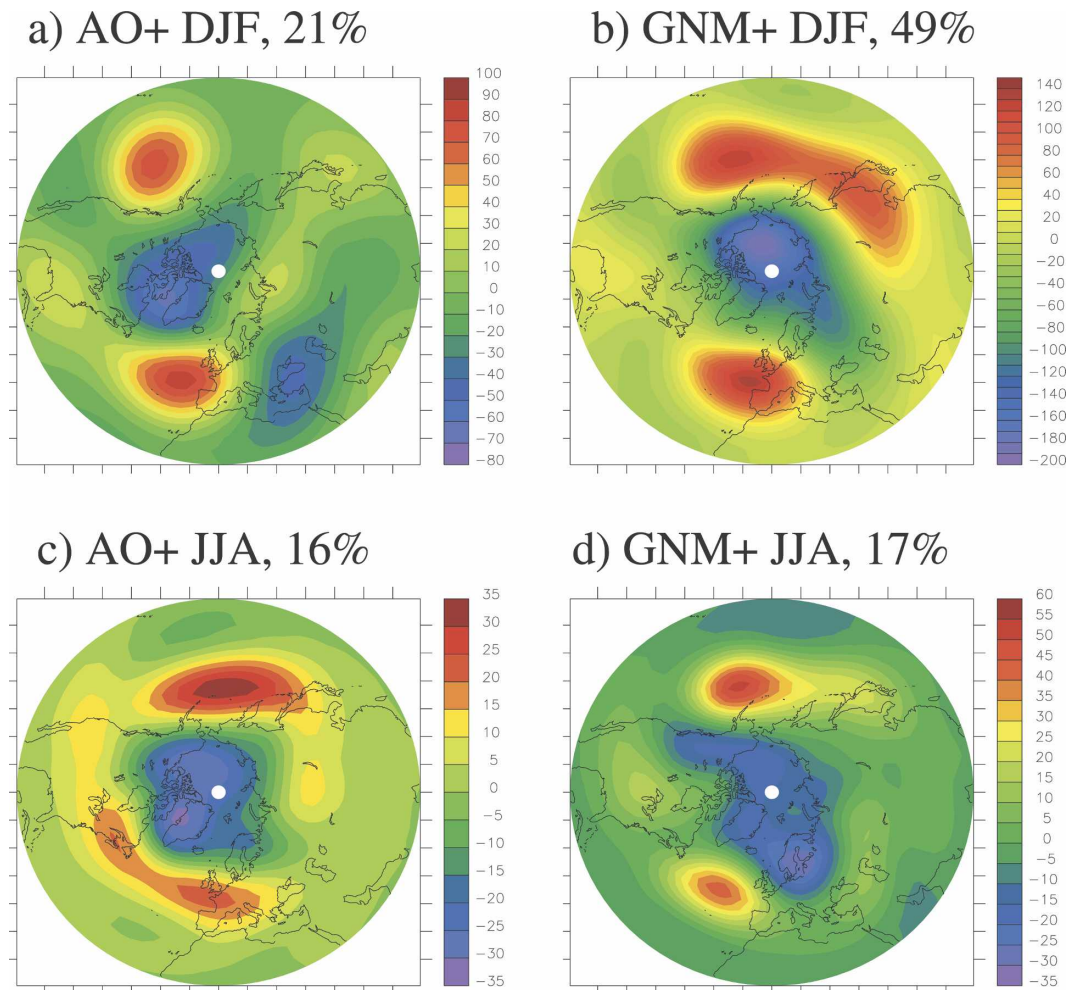


FIG. 3. AO/GNM based on monthly mean values ( $m$ ) in DJF for (a) MOD and (b) LGM simulations. (c), (d) Same as (a), (b) but for JJA. Number at the upper-right corner is the respective variance of the first EOF. The patterns are displayed as amplitudes by regressing hemispheric Z500 anomalies upon the standardized first principal component time series.

ences in the internal variability of the atmospheric flow, which may be dependent on the length of the time series applied in the EOF calculation. Turning to a discussion of the GNM in DJF (Fig. 3b), it is evident that substantial changes occur in this mode. Comparing the amplitude response of Z500 (Figs. 3a,b) it is clear that the AO significantly intensifies under LGM conditions. Moreover, the main center of action over Labrador/Greenland under modern conditions is shifted into the western Arctic Ocean under LGM conditions. The GNM also differs from modern over the Pacific Ocean; the main center of action under glacial conditions extends to eastern Asia, whereas in the MOD simulation it is confined to the northeastern Pacific. The AO in JJA reveals a different structure as compared to DJF (Fig. 3c). Under present-day conditions and during the positive phase of the AO, in midlatitudes a belt of high

pressure is clearly observed in the AO pattern, and the main centers of action are more zonally oriented (Fig. 3c). This is perhaps due to the interannual variability of SST and anomalous oceanic heat flux via the wind–evaporative–SST feedback (WES). High SST may induce an uplift of the Z500 surface associated with the expansion of the underlying air. Under LGM conditions (Fig. 3b), however, the main centers of action over the Atlantic and Pacific shrink as compared to winter conditions. The low pressure center over the Arctic region characteristic of DJF conditions also shifts to Scandinavia in JJA. This feature of the summer GNM is perhaps associated with a strong seasonal cycle that modulates the surface temperature in the Nordic Seas/Fennoscandia region (see Figs. 2c,d).

Turning to a similar investigation of the AAO in DJF (Figs. 4a,b), it is clear that the presence of glacial

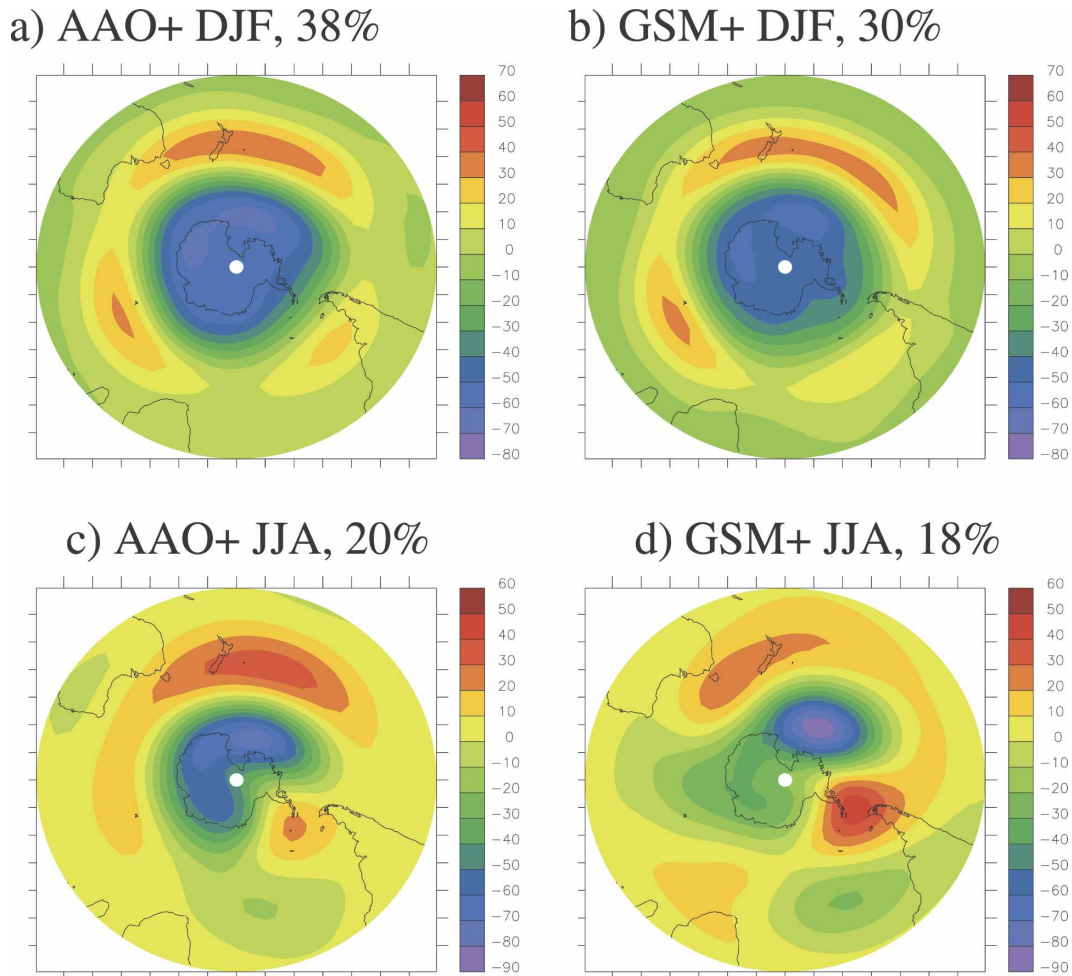


FIG. 4. As in Fig. 3 but for AAO/GSM.

boundary conditions does not result in an anomalous AAO during the LGM. As demonstrated by Justino and Peltier (2006) this mode is directly associated with SH climate symmetry, which is not significantly altered in the glacial climate in DJF compared to today (i.e., an annular structure is maintained). However, the AAO in JJA is characterized by a different structure as compared to DJF (Figs. 4c,d). It is important to note the departure of the AAO from the annular structure that is characteristic of present-day climate to a wavelike pattern under LGM conditions (Figs. 4c,d). Since the analyses of AAO/GSM have been described in Justino and Peltier (2006) there is no need to repeat this description here.

#### a. Northern Hemisphere response

In this section our goal is to explore the climate response associated with the positive phase of the AO for

both present-day and glacial climates. Positive (negative) phases of the AO are defined to correspond to periods when the time-evolving coefficient of the principal component of the first EOF is greater (less) than 0. We will not refer to these modes as Northern Hemisphere annular mode (NAM) and SAM because under glacial conditions they do cease to be characterized by an annular structure as shown previously.

Figures 5a and 5b show the response in surface temperature in DJF characteristic of the positive phase of the AO according to the predictions of the MOD and LGM simulations, respectively. The term “response” is here defined as the regression between hemispheric surface climate anomalies (e.g., temperature, wind, precipitation) upon the standardized first principal component time series. This pattern is hereafter named AO-TS. The positive (negative) phase of the AO is characterized by a stronger (weaker) than usual subtropical high pressure center and a deeper (shallower)

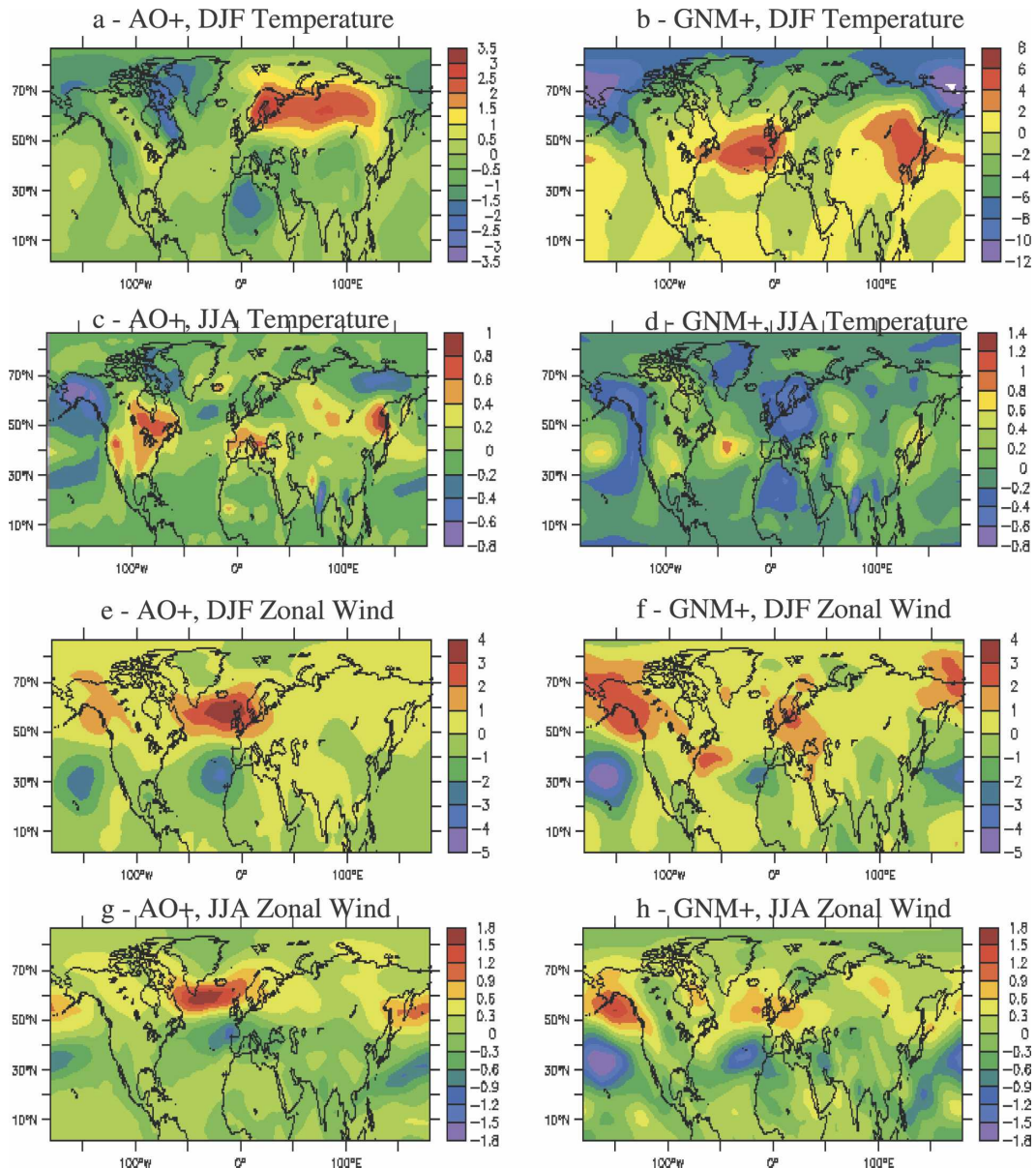


FIG. 5. Northern Hemisphere surface temperature response associated with the positive phase of AO/GNM in (a), (b) DJF and (c), (d) JJA. (e)–(h) Same as (a)–(d) but for zonal winds ( $\text{m s}^{-1}$ ). The left (right) panels are for MOD (LGM) simulation. The patterns are displayed as amplitudes ( $^{\circ}\text{C}$ ) by regressing hemispheric surface temperature anomalies upon the standardized first principal component time series. Please note that figures are shown with distinct labels.

than normal Icelandic low. Compared with previous composites based upon NCEP reanalyses (Wang et al. 2005; Thompson et al. 2003) our AO-TS (Fig. 5a) displays a high degree of similarity in both magnitude and spatial distribution. It is characterized by positive temperature response over Scandinavia and Eurasia, whereas colder conditions predominate over northeastern Canada and Greenland. Also of note is the cold region over northern Africa. The warmer conditions

over the northern Eurasian sector are a consequence of maritime air advection, as diagnosed by positive response of the westerly component of the wind (see Fig. 5e). On the other hand, due to a strengthening of the Azores high during the positive phase of the AO, anomalous extratropical air is advected to northern Africa, which in turn leads to the negative temperature response that occurs in this region.

Turning to the surface temperature response to the

GNM (GNM-TS; Fig. 5b), it is clear that under LGM conditions this mode is associated with a distinct temperature distribution as compared to present-day conditions with very large changes in magnitude. Most of the NH tropical region and the subtropics are dominated by positive GNM-TS, whereas high latitudes experience colder conditions (i.e., negative GNM-TS). During the positive phase of the GNM, the North Atlantic warms by 6°C as a result of less extensive sea ice extent along the Iberian coast. The relationship between the GNM and the sea ice extent has been discussed in Justino and Peltier (2005). The positive GNM-TS pattern over eastern Asia is linked to the advection of tropical air associated with the intensified high pressure system in the North Pacific.

It should be noted that this center of action in the LGM simulation is predicted to extend throughout the entire North Pacific basin (Fig. 3b). In addition, SLP response associated with the positive phase of the AO in the LGM simulation reaches values up to 12 hPa, whereas under modern conditions this response is approximately 4 hPa. The GNM-TS response north of 60°N does show an induced cooling marked by extremely cold conditions over the Bering Strait region. During NH summer (Figs. 5c,d), changes of the AO are expected to be related to warmer conditions over the east coast of North America, southern Europe, and East Asia. It is interesting to note that this pattern (Fig. 5c) is completely different from the AO-TS in winter (Fig. 5a). This warming is likely caused by an intensification of the meridional wind component (not shown) as demonstrated by regressing the leading PC of the AO upon the meridional wind anomalies (not shown). Strong meridional winds enhance warm temperature advection from the tropical region to midlatitudes, in particular over North America and East Asia. One should note that the primary contributor to the summer warming over North America is the radiative heating. Here we show only the contribution of the AO and GNM to surface temperature response.

Under LGM conditions, the GNM-TS (Fig. 5d) is characterized by well-defined node patterns over the North Atlantic and Scandinavia that appear to be associated with changes of sea ice and snow. Modifications in the albedo of sea ice and snow cover due to the seasonal changes of snowfall may induce differences in the regional pattern of surface temperature, in particular in the areas dominated by ice sheets. It should be stressed that northern Europe experiences an increase of cold-air advection from the sea ice-covered North Atlantic Ocean.

Figures 5e and 5f show zonal wind response in DJF

characteristic of positive phases of the AO and GNM. It is well known that the present-day AO is associated with strong midlatitude westerlies, which are more evident over the North Atlantic (Fig. 5e) as compared to the GNM counterpart. The GNM pattern (Fig. 5f) is also associated with zonal wind response over the North Atlantic. Over Eurasia, however, a different atmospheric flow configuration is expected to be characteristic of high latitudes. During NH summer, wind intensity and direction changes associated with the AO under modern conditions are weaker than during the winter season (Fig. 5g). It is still evident that the maximum westerly flow occurs over Scandinavia, whereas the northeastern trade winds dominate the NH tropics. Under LGM conditions the nature of the GNM-induced atmospheric flow (Fig. 5h) is modified as compared with modern conditions, in the sense that the area of enhanced westerlies is more confined over the North Atlantic and northeastern Pacific. Despite the weaker response compared to the North Atlantic counterpart, it should be mentioned that both modes AO and GNM affect the zonal atmospheric circulation over the North Pacific.

#### *b. Southern Hemisphere response*

Turning to the surface temperature response induced by vacillations of the AAO/GSM (Figs. 6a,b), it is clear that during the positive phase of the AAO the subtropical (polar) region experiences slightly warmer (colder) conditions. Over the ocean these changes mainly reflect changes of SST. During the positive phase of the AAO, weaker (stronger) westerlies are predicted to occur in the vicinity of 30°–45°S (45°–60°S) (see Figs. 6e,f), which in turn reduces (intensifies) the total heat loss from the ocean to the atmosphere via the WES feedback. This might be associated with warmer surface conditions (i.e., positive AAO-TS/GSM-TS). Farther south, as discussed by Hall and Visbeck (2002), the associated Ekman drift generates anomalous upwelling along the margins of the Antarctic continent, thus leading to colder surface temperature. Comparing Fig. 6a with Fig. 6b, it turns out that the presence of glacial boundary conditions does not result in significant changes of the GSM-TS as compared to this pattern under present-day conditions. This can be expected since there is no substantial modification to the form and intensity of the GSM as compared to modern conditions (Fig. 4).

Surface temperature response induced by the AAO variability in JJA is shown in Figs. 6c and 6d. This figure resembles the Antarctic dipole as defined by Yuan and Martinson (2000), which is characterized by a zonal see-

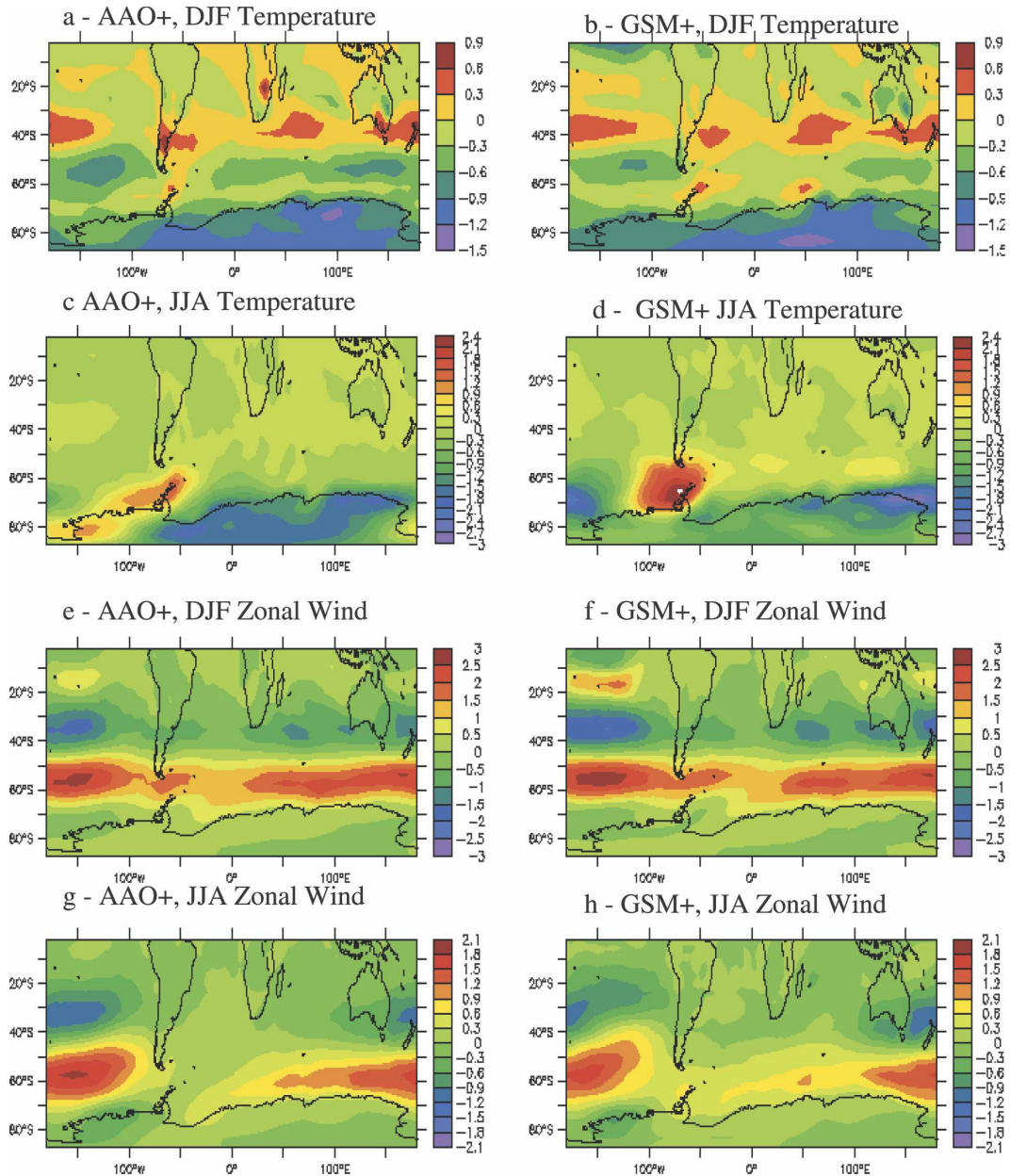


FIG. 6. Same as in Fig. 5 but for Southern Hemisphere.

saw in surface temperature, as well as other indices, between the eastern Pacific and Atlantic sectors of the Antarctic region. In the modern simulation colder conditions are also evident over the Antarctic mainland (Fig. 6c). The most interesting feature, however, appears over the Antarctic Peninsula, where positive surface temperature response dominates. Similar warming has been detected by van den Broeke and van Lipzig (2004) and Thompson and Solomon (2002). The latter study suggested that the warming found in observations could be taken to indicate a trend toward stronger cir-

cumpolar flow. Figure 6d shows that in the LGM simulation the Antarctic Peninsula warming is intensified by a factor of 2, as expected due to increased temperature advection of warm air from the extratropical region (not shown).

Except for slightly enhanced zonal flow over the Drake Passage under glacial conditions, analyses for the SH (Figs. 6e–h) do not reveal substantial changes of the circumpolar flow between the present day and LGM. One may note, however, seasonal changes do exist in which the zonal flow characteristic of summer

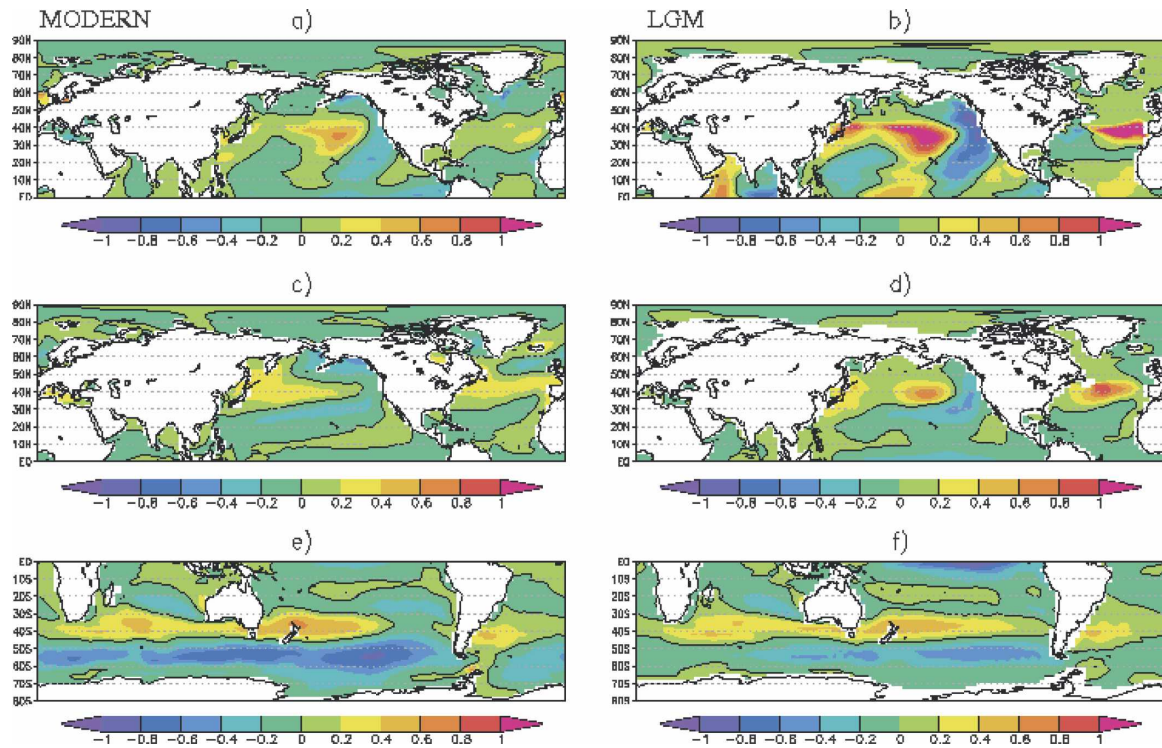


FIG. 7. Present-day SST response ( $^{\circ}\text{C}$ ) associated with the positive phase of AO/GNM in (a) DJF and (c) JJA. (b), (d) Same as (a), (c) but for LGM conditions. (e) Present-day SST response due to the positive phase of AAO in DJF; (f) same as (e) but for GSM.

conditions show a wavy-like structure in JJA. This initial evaluation demonstrates that insofar as surface temperature and zonal wind are concerned, the glacial simulation delivers larger differences in the variability fields, due to vacillation of the GNM and GSM than predicted for present-day conditions. This was not anticipated because, in the LGM experiment, a large fraction of the earth's surface in the extratropics is ice covered throughout the year. Therefore, seasonal changes of the diabatic forcing linked to ice–albedo feedback are expected to be weaker in comparison with modern conditions.

Changes of precipitation associated with the modern AO, AAO, GNM, and GSM (not shown) in both seasons are very small. It should be noted, however, that positive AO phases induce an intensification of the Indian monsoon under present-day and glacial conditions. Gong and Ho (2003) have also noted that the summer AO index is quite well correlated with summer Asian rainfall. In the SH, the main pattern associated with the AAO/GSM reveals many similarities with the precipitation anomalies that are characteristic of La Niña events (Ropelewski and Halpert 1987). Moreover, the AAO seems to lead in general to wetter (drier) conditions around the Antarctic continent (mid-latitudes).

### c. Oceanic response

As might be expected, the AO/GNM and AAO/GSM induced changes of surface temperature and atmospheric circulation lead to anomalous oceanic surface conditions. In this section of the paper the impact of these modes on SST, the meridional overturning circulation (MOC), and Ekman dynamics via Sverdrup transport are addressed. The influence of the surface westerlies in the lower troposphere on SST was first described in the early literature by Bjerknes (1964). He found that strong westerly flow, perhaps associated with positive phases of the AO, leads to warmer SST in the western portion of the North Atlantic between  $30^{\circ}$  and  $45^{\circ}$ , whereas colder temperatures are found in the subpolar region. Recently, Marshall et al. (2001) and Seager et al. (2000) have provided additional support for Bjerknes' finding in terms of the spatial pattern. Their work has, however, suggested smaller amplitude anomalies.

Figure 7 shows the SST response in DJF and JJA induced by the positive phase of AO/GNM and AAO/GSM for both present-day and LGM conditions as simulated by the CSM. Clearly evident (Fig. 7a) is the SST tripole in the North Atlantic with positive SST response between  $30^{\circ}$ – $50^{\circ}\text{N}$ , which are bounded by

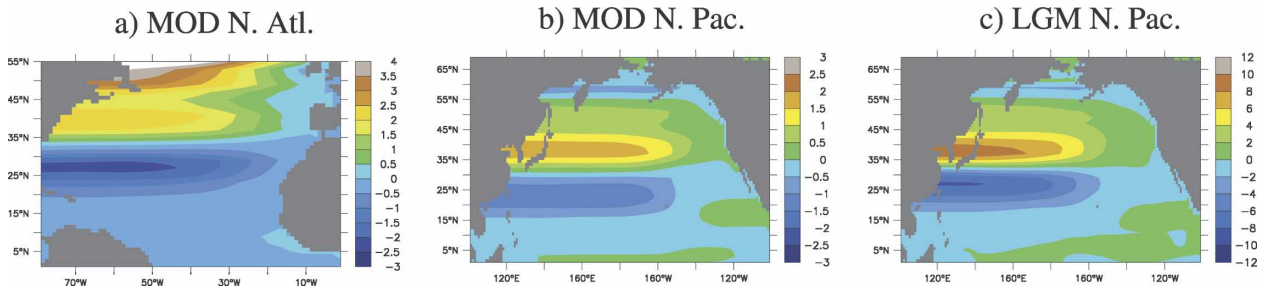


FIG. 8. (a) Winter mean (DJF) Sverdrup transport anomalies (Sv) in the North Atlantic for present-day conditions associated with the AO. (b) Same as (a) but for North Pacific. (c) Sverdrup transport anomalies under LGM conditions induced by the positive phases of the GNM. Positive values correspond to anticyclonic circulation, whereas negative values are associated with cyclonic circulation.

negative SST response to the north and south. Our MOD simulation predicts amplitudes from  $+0.5$  to  $-0.6^{\circ}\text{C}$  (Fig. 7a). This is in the range of covariance values inferred by Visbeck et al. (2003) based on 100 yr of observed SST anomaly data and the North Atlantic Oscillation (NAO) index. Although there are many uncertainties concerning the climate mechanisms that support the tripole, some light has been shed on the relevance of air–sea heat fluxes as an important agent, especially far from coastal regions (Visbeck et al. 2003; Seager et al. 2000). One may note that any change in the meridional position of the SST tripole would have a substantial impact upon the position of the intertropical convergence zone (ITCZ) and therefore on tropical precipitation. In addition to changes in local oceanic heat content, the atmospheric forcing associated with the AO also leads to modifications of the wind-driven circulation. This is diagnosed by calculation of the Sverdrup transport (Fig. 8). The Sverdrup transport is defined as

$$\psi(x) = \frac{1}{\beta\rho} \int_{x_e}^x \frac{\partial\tau_x}{\partial y} dx, \quad (1)$$

where  $\beta$  is the usual meridional derivative of the Coriolis parameter,  $\rho$  is the mean density of seawater, and  $\tau_x$  is the zonal component of the wind stress. Here,  $X$  and  $X_e$  are the locations of the eastern and western boundaries in the ocean basin. Based on Fig. 8 it is clear that an enhanced anticyclonic (cyclonic) circulation of 3–4 Sverdrups (Sv; where  $1 \text{ Sv} \equiv 10^6 \text{ m}^3 \text{ s}^{-1}$ ) is located between  $30^{\circ}$ – $60^{\circ}\text{N}$  ( $20^{\circ}$ – $30^{\circ}\text{N}$ ). One may argue that there exists an intensification of the subtropical gyre in which the advection of tropical water embedded in the gyre is perhaps another source for positive SST response as shown in Fig. 7a. This result is somehow different than suggested by previous investigations (Visbeck et al. 2003; Marshall et al. 2001) that propose the existence of a unique gyre, the so-called intergyre gyre. We do not show the GNM-induced Sverdrup transport

response in the North Atlantic as predicted by the LGM simulation because this area is essentially covered by perennial sea ice.

SST response associated with the AO variability is also notable in the North Pacific. This pattern (Fig. 7a) resembles the cool phase of the PDO (Latif and Barnett 1994), which is characterized by warmer (colder) conditions than normal in the central North (eastern) Pacific. The AO-induced SST response corresponds to 60% of the SST anomalies associated with our PDO pattern based on the first EOF of SST in the North Pacific (not shown). Similarly, the Sverdrup transport response in the North Atlantic and the North Pacific is associated with an intensification of the subtropical gyre and of the subpolar gyre during the positive phase of the AO. This favors a surface warming in the Kuroshio area and the central North Pacific, whereas the enhanced supply of cold water from the subpolar gyre leads to a colder eastern Pacific. Furthermore, the poor WES feedback due to a weaker subtropical jet (Fig. 5e) is another source of warming.

Turning to LGM conditions (Fig. 7b), in spite of the substantial changes in the AO that occur under glacial conditions (GNM pattern), this does not result in a modification of the SST spatial distribution as compared with the present-day AO-induced SST pattern. There do exist, however, substantial changes in the magnitude of the response. In the eastern Atlantic, during the positive phases of the GNM, a retreat of the sea ice front occurs, which leads to higher SST response by up to  $1^{\circ}\text{C}$ . An intensification of SST response due to the GNM is also found in the North Pacific, a finding that is in agreement with changes in surface winds (Fig. 5f) and Sverdrup transport (Fig. 8c). Figures 7c and 7d demonstrate that the SST response in JJA is similar to their winter counterparts but of smaller amplitude. This is reasonable since the AO/GNM together with its climate impact is much weaker in the summer season.

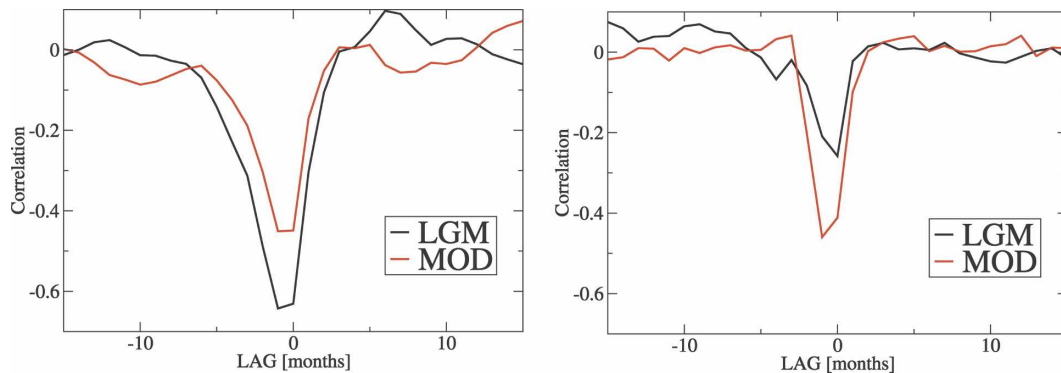


FIG. 9. Lag correlation coefficient between the first PC of the AO/GNM and the PDO for MOD (black) and LGM (red) simulations; (left) DJF and (right) JJA (see text for details).

Changes of SST in the SH are influenced by the AAO/GSM, as shown in Figs. 7e and 7f. The impact of the AAO on SST during DJF can be summarized as a midlatitude warming around  $45^{\circ}\text{S}$  and a cooling in the Antarctic circumpolar region. According to Hall and Visbeck (2002) this warming-cooling seesaw is tied to changes of the wind stress due to vacillation of the AAO. In fact, wind stress changes lead to modification of Ekman-driven surface conditions. Comparing the present day and the LGM SST response due to the AAO and GSM, it turns out that in summer (Figs. 7e,f) both patterns are very similar despite the increase in sea ice under glacial conditions. Moreover, this may be taken to suggest that there is no change in the position of the main wind pattern. It is important to note the warm response that occurs in the South Atlantic under both boundary conditions.

Although the magnitude of the response is smaller as compared to DJF, the SST changes related to the AAO in JJA depend upon the boundary conditions (not shown). The dominant characteristic that distinguishes the present day from the glacial SST response associated with the positive phase of the AAO/GSM is, however, the intensification of SST response in the equatorial/tropical Pacific under LGM conditions. As demonstrated by Justino and Peltier (2006), the leading PC of SST in the tropical Pacific and the GSM are significantly correlated, perhaps suggesting that the tropical-extratropical teleconnection was enhanced during the LGM period.

Changes of atmospheric and oceanic circulations and sea ice extent have a large impact on processes driving deep-water formation and thereby on the MOC. At present there is no established theory as to how atmospheric changes impact the dynamics of the MOC. As emphasized by Schmitt et al. (1989) and Speer and Tziperman (1992), surface density anomalies (a combination of the anomalies due to temperature and salinity

changes) can generate changes in the strength of the MOC. A brief investigation of these density changes predicted by the MOD and LGM simulations may therefore be expected to reveal whether or not a positive phase of the AO would be associated with a weaker MOC, due to increased precipitation and the attendant de-densification of surface waters, which inhibits convection in the main sites of deep-water formation. As argued by Schmitt et al. (1989), the salinity might be expected to dominate the density flux at the ice-water interface where the deep convection takes place. The proposed out-of-phase relationship between the AO and the MOC (stronger AO-weak MOC) was confirmed by Peltier and Solheim (2002) and Justino and Peltier (2005) for both present-day and LGM conditions. Based on modeling results, Paiva and Chassignet (2002) also found enhanced (weaker) transport at  $55^{\circ}\text{N}$  in the Deep Western Boundary Current during periods of low (high) NAO index. Häkkinen (1999) has proposed that the induced changes of the MOC to NAO/AO variability are regionally dependent. She argued that the strength of the MOC increases by about 3 Sv for positive NAO/AO index at  $25^{\circ}\text{N}$  but that it decreases north of  $45^{\circ}\text{N}$ . Studies showing that both patterns vary in phase, however, do exist (e.g., Visbeck et al. 2003; Carsten and Jung 2001). Recently, Bryden et al. (2005), based on measurements from ships on a transatlantic section along latitude  $25^{\circ}\text{N}$ , suggest that the Atlantic MOC has slowed by about 30%, mostly between 1957 and 2004. It should be noted that during this period more frequent positive AO index has been measured. This suggests that the interplay between the MOC and the AO may perhaps be model dependent and that further and more study is needed to clarify the dynamic mechanisms associated with these modes of climate variability.

In what follows, the interaction between the AO and PDO is briefly discussed based on correlation and

spectral analyses. Latif (2006), investigating the North Pacific multidecadal variability, argued that the nature of the North Pacific climate perhaps resides in the uncoupled (atmosphere–ocean) regime; that is, the multidecadal dynamical ocean changes are mainly due to stochastic wind stress forcing. By analyzing the PC time series of the AO and PDO we have found, however, that the ocean and atmosphere in the North Pacific are significantly anticorrelated. Figure 9 shows that there is no significant seasonal difference in the correlation between the PDO and AO under modern conditions; on the other hand, they are stronger anticorrelated in DJF than in JJA in the glacial simulation. This might be associated with an intensification of the LGM atmospheric flow during the winter season (Fig. 5f), which in turn induces oceanic changes via Ekman dynamics and air–sea flux exchange (Fig. 8c). Given this one may argue that the coupling between the North Pacific and the overlying atmosphere is highly dependent on the strengthening and spatial distribution of the atmospheric forcing.

Furthermore, spectral analyses reveal that both the PDO and the AO support a multidecadal mode characterized by a time scale near 35 yr. This feature is stronger under modern than under LGM conditions (not shown). The substantial increase of sea ice in the glacial simulation seems to be responsible for the diminution of power associated with the glacial PDO and AO.

#### 4. Conclusions

Based upon 2500-yr-long coupled climate simulations driven by present-day and glacial boundary conditions we have investigated the impact of the Arctic Oscillation (AO) and Antarctic Oscillation (AAO) on the earth's climate. It has been demonstrated that significant changes of surface conditions are predicted to occur in both epochs depending upon the phase of the AO and AAO. Moreover, these climate responses differ substantially from modern to LGM conditions and exhibit a strong seasonal cycle (Figs. 5, 6). For instance, during the positive phase of the glacial northern mode (GNM), surface temperature response can achieve an amplitude as large as 10°C in the Arctic region, whereas the North Atlantic and eastern Asia warm by as much as 5°C. Under present-day conditions the amplitude of this response is reduced by a factor of 3. The SH also experiences systematic climate shifts due to variations of the Antarctic Oscillation/Glacial Southern Mode; the most important of these shifts consists of a warming over the Antarctic Peninsula and midlatitudes (Fig. 6) during the positive phase of the AAO/GSM.

We have furthermore demonstrated that vacillations of the AO/GNM and AAO/GSM also lead to changes of surface ocean conditions. Air–sea fluxes of heat and momentum as well as wind-driven circulation Ekman dynamics are tightly linked to these modes of climate variability through midlatitude westerlies and tropical easterlies. Based on Sverdrup transport calculations it has been shown that an intensification of the subtropical gyres in both the North Atlantic and North Pacific play a key role in the development of positive SST response in midlatitudes during the positive phase of the AO. This SST pattern is intensified under LGM conditions due to the stronger GNM (Figs. 7a,b) that exists at this time. In the SH extratropics, the atmosphere–ocean interaction during the positive phase of the AAO can be summarized as consisting of Ekman-driven upwelling along the Antarctic continent. Therefore, lower SST is found in the Antarctic Circumpolar Current region, whereas the midlatitudes experience larger SST response due to weaker westerlies. This is consistent with the previous analyses of Lefebvre et al. (2004) and Hall and Visbeck (2002).

Computation of the lagged correlation between the first PC of the AO and the corresponding PC of SST in the North Pacific, which represents the time variability of the Pacific decadal oscillation, shows that the PDO and AO are significantly anticorrelated. Under present-day conditions this coupling does not seem to be seasonally dependent. In contrast, under glacial conditions the coupling is stronger during the boreal winter season mainly due to increased wind forcing. The AO-induced SST changes in the North Pacific, at least in our experiments, account for nearly 60% of the variability of SST as reproduced by the PDO.

#### REFERENCES

- Bettge, T. W., J. Weatherly, W. Washington, D. Pollard, B. Briegleb, and W. G. Strand, 1996: The NCAR CSM Sea Ice Model. NCAR Tech. Note TN-425+STR, 25 pp.
- Bjerknes, J., 1964: Atlantic air–sea interaction. *Advances in Geophysics*, Vol. 10, Academic Press, 1–82.
- Bonan, G., 1998: The land surface climatology of the NCAR Land Surface Model (LSM 1.0) coupled to the NCAR Community Climate Model (CCM3). *J. Climate*, **11**, 1307–1326.
- Broccoli, A., and S. Manabe, 1987: The influence of continental ice, atmospheric CO<sub>2</sub>, and land albedo on the climate of the last glacial maximum. *Climate Dyn.*, **1**, 87–99.
- Bryden, H. L., H. R. Longworth, and S. A. Cunningham, 2005: Slowing of the Atlantic meridional overturning circulation at 25°N. *Nature*, **438**, 655–657.
- Cai, W., G. Shi, and Y. Li, 2005: Multidecadal fluctuations of winter rainfall over southwest Western Australia simulated in the CSIRO Mark 3 coupled model. *Geophys. Res. Lett.*, **32**, L12701, doi:10.1029/2005GL022712.
- Carsten, E., and T. Jung, 2001: North Atlantic interdecadal vari-

- ability: Oceanic response to the North Atlantic Oscillation (1865–1997). *J. Climate*, **14**, 676–691.
- Carvalho, L. M. V., C. Jones, and T. Ambrizzi, 2005: Opposite phases of the Antarctic Oscillation and relationships with intraseasonal to interannual activity in the Tropics during the austral summer. *J. Climate*, **18**, 702–718.
- CLIMAP, 1981: *Seasonal Reconstruction of the Earth's Surface of the Last Glacial Maximum*. Geological Society of America Map and Chart Series, No. 36, 1–18.
- Cook, E., 2003: Multi-proxy reconstructions of the North Atlantic Oscillation (NAO) index: A critical review and a new well-verified winter NAO index reconstruction back to AD 1400. *The North Atlantic Oscillation, Geophys. Monogr.*, Vol. 134, Amer. Geophys. Union, 63–79.
- , R. D. D'Arrigo, and K. R. Briffa, 1998: A reconstruction of the North Atlantic Oscillation using tree-ring chronologies from North America and Europe. *The Holocene*, **8**, 9–17.
- Farrera, I., and Coauthors, 1999: Tropical climates at the Last Glacial Maximum: A new synthesis of terrestrial palaeoclimate data. *Climate Dyn.*, **15**, 823–856.
- Gong, D.-Y., and S. Wang, 1999: Definition of Antarctic oscillation index. *Geophys. Res. Lett.*, **26**, 459–462.
- , and C.-H. Ho, 2003: Arctic oscillation signals in the East Asian summer monsoon. *J. Geophys. Res.*, **108**, 4066, doi:10.1029/2002JD002193.
- Häkkinen, S., 1999: Variability of the simulated meridional heat transport in the North Atlantic for the period 1951–1993. *J. Geophys. Res.*, **104**, 10 991–11 008.
- Hall, A., and M. Visbeck, 2002: Synchronous variability in the Southern Hemisphere atmosphere, sea ice, and ocean resulting from the annular mode. *J. Climate*, **15**, 3043–3057.
- Hurrell, J. W., 1995: Decadal trends in the North Atlantic Oscillation: Regional temperatures and precipitation. *Science*, **269**, 676–679.
- Justino, F., and W. R. Peltier, 2005: The glacial North Atlantic Oscillation. *Geophys. Res. Lett.*, **32**, L21803, doi:10.1029/2005GL023822.
- , and —, 2006: Influence of present day and glacial surface conditions on the Antarctic Oscillation/Southern Annular Mode. *Geophys. Res. Lett.*, **33**, L22702, doi:10.1029/2006GL027001.
- , A. Timmermann, U. Merkel, and E. Souza, 2005: Synoptic reorganization of atmospheric flow during the Last Glacial Maximum. *J. Climate*, **18**, 2826–2846.
- Kiehl, J. T., J. Hack, G. Bonan, B. Boville, D. Williamson, and P. Rasch, 1998: The National Center for Atmospheric Research Community Climate Model: CCM3. *J. Climate*, **11**, 1131–1149.
- Kim, S., G. Flato, and G. Boer, 2003: A coupled climate model simulation of the Last Glacial Maximum, Part 2: Approach to equilibrium. *Climate Dyn.*, **20**, 635–661.
- Kushner, P. J., I. M. Held, and T. L. Delworth, 2001: Atmospheric circulation response to global warming. *J. Climate*, **14**, 2238–2249.
- Latif, M., 2006: On North Pacific multidecadal climate variability. *J. Climate*, **19**, 2906–2915.
- , and T. Barnett, 1994: Causes of decadal climate variability over the North Pacific and North America. *Science*, **266**, 634–637.
- Lefebvre, W., H. Goosse, R. Timmermann, and T. Fichefet, 2004: Influence of the Southern Annular Mode on the sea ice-ocean system. *J. Geophys. Res.*, **109**, C09005, doi:10.1029/2004JC002403.
- Levitus, S., 1982: *Climatological Atlas of the World Ocean*. NOAA Prof. Paper 13, 173 pp. and 17 microfiche.
- Manabe, S., and A. Broccoli, 1985: The influence of continental ice sheets on the climate of an ice age. *J. Geophys. Res.*, **90**, 2167–2190.
- Marshall, J., H. Johnson, and J. Goodman, 2001: A study of the interaction of the North Atlantic Oscillation with ocean circulation. *J. Climate*, **14**, 1399–1421.
- Nakano, H., R. Furue, and N. Suginoara, 1999: Effect of seasonal forcing on global circulation in a world ocean general circulation model. *Climate Dyn.*, **15**, 491–502.
- Paiva, M. A., and E. P. Chassignet, 2002: North Atlantic modeling of low-frequency variability in mode water formation. *J. Phys. Oceanogr.*, **32**, 2666–2680.
- Peltier, W. R., 1994: Ice age paleotopography. *Science*, **265**, 195–201.
- , and L. P. Solheim, 2002: Dynamics of the ice age Earth: Solid mechanics and fluid mechanics. *J. Phys. IV*, **12**, 85–104.
- , and —, 2004: The climate of the Earth at Last Glacial Maximum: Statistical equilibrium state and a mode of internal variability. *Quat. Sci. Rev.*, **23**, 335–357.
- Peyron, O., and Coauthors, 2005: Late-Glacial climatic changes in Eastern France (Lake Lautrey) from pollen, lake-levels, and chironomids. *Quat. Res.*, **64**, 197–211.
- Pflaumann, U., and Coauthors, 2003: Glacial north Atlantic: Sea-surface conditions reconstructed by GLAMAP 2000. *Paleoceanography*, **18**, 1065, doi:10.1029/2002PA000774.
- Rind, D., 1987: Components of the ice age circulation. *J. Geophys. Res.*, **92**, 4241–4281.
- Rodwell, M. J., D. P. Rowell, and F. K. Folland, 1999: Oceanic forcing of the wintertime North Atlantic Oscillation and European climate. *Nature*, **398**, 320–323.
- Rogers, J. C., 1990: Patterns of low-frequency monthly sea-level pressure variability (1899–1986) and associated wave cyclone frequencies. *J. Climate*, **3**, 1364–1379.
- Ropelewski, C. H., and S. Halpert, 1987: Global and regional scale precipitation patterns associated with the El Niño/Southern Oscillation. *Mon. Wea. Rev.*, **115**, 1606–1626.
- Schmitt, R., P. Bogden, and C. Dorman, 1989: Evaporation minus precipitation and density fluxes for the North Atlantic. *J. Phys. Oceanogr.*, **19**, 1208–1221.
- Seager, R., Y. Kushnir, M. Visbeck, N. H. Naik, J. Miller, G. Krahnmann, and H. Cullen, 2000: Causes of Atlantic Ocean climate variability between 1958 and 1998. *J. Climate*, **13**, 2845–2862.
- Shin, S.-I., Z. Liu, B. Otto-Bliesner, E. Brady, J. Kutzbach, and S. Harrison, 2003: A simulation of the Last Glacial Maximum climate using the NCAR–CSM. *Climate Dyn.*, **20**, 127–151.
- Silvestri, G., and C. Vera, 2003: Antarctic Oscillation signal on precipitation anomalies over southeastern South America. *Geophys. Res. Lett.*, **30**, 2115, doi:10.1029/2003GL018277.
- Speer, K., and E. Tziperman, 1992: Rates of water mass formation in the North Atlantic Ocean. *J. Phys. Oceanogr.*, **22**, 94–104.
- Tarasov, P., and Coauthors, 1999: Last Glacial Maximum climate of the former Soviet Union and Mongolia reconstructed from pollen and plant macrofossil data. *Climate Dyn.*, **15**, 227–240.
- Thompson, D. W. J., and J. M. Wallace, 1998: The Arctic Oscillation signature in the wintertime geopotential height and temperature fields. *Geophys. Res. Lett.*, **25**, 1297–1300.
- , and —, 2000: Annular modes in the extratropical circulation. Part I: Month-to-month variability. *J. Climate*, **13**, 1000–1016.

- , and —, 2001: Regional climate impacts of the Northern Hemisphere annular mode. *Science*, **293**, 85–89.
- , and S. Solomon, 2002: Interpretation of recent Southern Hemisphere climate change. *Science*, **296**, 895–899.
- , S. Lee, and M. P. Baldwin, 2003: Atmospheric processes governing the Northern Hemisphere Annular Mode/North Atlantic Oscillation. *The North Atlantic Oscillation, Geophys. Monogr.*, Vol. 134, Amer. Geophys. Union, 81–112.
- van den Broeke, M. R., and N. P. M. van Lipzig, 2004: Changes in Antarctic temperature, wind and precipitation in response to the Antarctic Oscillation. *Ann. Glaciol.*, **39**, 119–126.
- Vettoretti, G., W. R. Peltier, and N. A. McFarlane, 2000: Global water balance and atmospheric water vapour transport at Last Glacial Maximum: Climate simulations with the CCCma atmospheric general circulation model. *Can. J. Earth Sci.*, **37**, 695–723.
- Visbeck, M., E. P. Chassignet, R. G. Curry, T. L. Delworth, R. R. Dickson, and G. Krahmann, 2003: *The Oceans Response to North Atlantic Oscillation Variability*. Amer. Geophys. Union.
- Wallace, J. M., and D. Gutzler, 1981: Teleconnections in the geopotential height field during the Northern Hemisphere winter. *Mon. Wea. Rev.*, **109**, 784–812.
- Wang, D., C. Wang, X. Yang, and J. Lu, 2005: Winter Northern Hemisphere surface air temperature variability associated with the Arctic Oscillation and North Atlantic Oscillation. *Geophys. Res. Lett.*, **32**, L16706, doi:10.1029/2005GL022952.
- Xie, T., and C. Arkin, 1997: Global precipitation: A 17-year monthly analysis based on gauge observations, satellite estimates, and numerical model outputs. *Bull. Amer. Meteor. Soc.*, **78**, 2539–2558.
- Yuan, X. J., and D. G. Martinson, 2000: Antarctic sea ice extent variability and its global connectivity. *J. Climate*, **13**, 1697–1717.